Wheel-Load Distribution Results from AISI-FHWA Model Bridge Study

MARK MOORE, KARL A. STRAND, MICHAEL A. GRUBB, AND LLOYD R. CAYES

An experimental test program to evaluate the behavior of a 0.4-scale model of a two-span continuous plate-girder bridge with modular precast prestressed concrete deck panels has recently been completed. The bridge, designed according to Alternate Load Factor Design (ALFD), or Autostress Design, procedures, utilizes noncompact plate girders with slender webs that fall beyond the present limits of the ALFD guide specification. A comprehensive plan was followed to subject the model to a series of tests to evaluate specific responses at simulated AASHTO service load, overload, and maximum load levels. At elastic service-load stress levels, live-load lateral-distribution factors were computed from experimentally developed influence surfaces. These factors were compared with factors computed from a finite-element model, from current AASHTO procedures, and from proposed empirical formulas. The factors computed from the experimental and finite-element model data were generally in close agreement. The factors computed from the proposed empirical formulas for the interior girder also agreed closely with the experimental data. The factors computed using AASHTO procedures were quite conservative for the interior girder and less so for the exterior girders. Neither the proposed nor the current AASHTO procedures were found to account for the observed slight variation of the distribution factor along the span. The data would seem to indicate that finite-element analysis and the proposed empirical formulas are both plausible methods for computing elastic girder wheel-load distribution factors. For similar tests conducted after the formation of automoments along with subsequent shakedown at overload, the computed distribution factors varied less than 10 percent. Thus it appears that elastic distribution factors may still be used at overload, even though controlled local yielding is allowed in ALFD procedures. In addition, for similar tests conducted with selected cross-frames removed, changes in the computed distribution factors were less than 10 percent in the positive-moment region for both interior and exterior girders. For the interior girder in the negative-moment region, distribution factors varied up to an average of 15 percent for the tests conducted with cross-frames in place and with selected cross-frames removed. This suggests that the load was distributed primarily through the concrete deck.

In 1982 a jointly funded bridge research program was initiated between the American Iron and Steel Institute (AISI) and the Federal Highway Administration (FHWA). The primary purpose of the large experimental test program was to study experimentally the behavior of a scale model of a two-span continuous plate-girder bridge designed according to Alternate Load Factor Design (ALFD), or Autostress Design, procedures (*1*) and built with modular precast prestressed concrete deck panels. In ALFD, a designer is permitted to utilize some of the substantial postyielding reserve strength that is available in continuous plate-girder bridges. Currently, an AASHTO guide specification (*2*) permits the use of ALFD for the design of continuous bridges using rolled-beam and comparable welded-beam sections that satisfy specific compactness requirements. As part of an ongoing research program to extend the ALFD procedures to noncompact sections, the model bridge test was designed using plate-girder sections that do not satisfy the current compactness requirements of the ALFD specification.

Testing of the model bridge included the development of elastic influence surfaces for the computation of lateral live-load distribution factors for interior and exterior girders in positive and negative bending at AASHTO service load levels. The three-dimensional influence surfaces were computed for selected reactions, moments, and shears in the model bridge (*3*). Three-dimensional influence surfaces were also developed for measured axial forces in the bottom flange of selected girders. These bottom-flange forces, which are a measure of the bending moment in the girder, were then used to compute lateral distribution factors. Initially, tests placed at specific locations to determine these elastic influence surfaces for a single concentrated load were completed. These tests were conducted immediately following construction of the model bridge. Following the completion of testing at the AASHTO overload level, in which controlled local yielding and subsequent shakedown were observed in the girders after several cycles of simulated overload live load plus impact, these influence surfaces were developed again. The influence surfaces were also developed by repeating the tests with selected cross-frames removed.

This paper provides a summary of these three influence surface tests. Live-load distribution factors computed from the experimental data are compared with factors computed using a mathematical finite-element model, current AASHTO procedures, and empirical formulas and recommendations recently developed as part of National Cooperative Highway Research Program (NCHRP) Project 12-26 on lateral live-load distribution.

M. Moore and K. A. Strand, Wiss, Janney, Elstner Associates, Inc. 3100 Premier Drive, Suite 200, Irving, Tex. 78063. M. A. Grubb, AISC Marketing, Inc., 650 Smithfield Street, Suite 750, Pittsburgh, Pa. 15222-3907. L. R. Cayes, Federal Highway Administration, 6300 Georgetown Pike, HNR-10, McLean, Va. 22101.

BACKGROUND OF MODEL BRIDGE STUDY

The model bridge study is part of an extensive research program in progress to extend the ALFD concepts to noncompact plate-girder sections with slender webs that fall outside the compactness limits of the current ALFD guide specification (*4–8*). The experimental study involved the laboratory testing of a 0.4-scale model of a two-span continuous plate-girder highway bridge. The prototype bridge was designed by industry personnel using ALFD procedures. The model bridge consisted of two 56-ft spans, each with three plate girders. The girders supported 4-in.-thick modular precast concrete deck panels made composite with the plate girders using stud shear connectors. The panels were prestressed both transversely and parallel to the bridge axis. Components for the bridge were fabricated in two commercial shops and erected by a steel fabricator in the FHWA Structures Laboratory at the Turner Fairbank Highway Research Center in McLean, Virginia. Construction of the model bridge was completed in April 1987.

A comprehensive test plan was developed with the objective of evaluating specific responses of the model bridge at each of the three load levels specified by AASHTO—service load, overload, and maximum load. These load levels are used in ALFD and in the current AASHTO limit-states design approach known as Load Factor Design (LFD) (*9*). In both LFD and ALFD, specific structural performance requirements must be satisfied at each of the three load levels.

DESCRIPTION OF MODEL BRIDGE

Design of the model bridge began with design of a full-scale prototype. The prototype was designed according to ALFD procedures. The prototype bridge configuration used was a two-span continuous structure with equal spans of 140 ft. Overall deck width was 48 ft. The roadway width of 44 ft 6 in. allowed for three design lanes. The deck consisted of uniform 10-in.-thick precast concrete panels 8 ft wide by 48 ft long.

The superstructure consisted of three parallel flange (68-in. web depth) steel plate girders spaced at 17 ft, with a deck overhang beyond the exterior girders of 7 ft. Unpainted ASTM A588 weathering steel, 50 ksi nominal yield, was assumed in the design. Because the prototype bridge girders were designed using ALFD procedures, it was possible to use a prismatic girder section over the interior pier for this particular bridge configuration.

The bridge was designed for AASHTO HS-20 live loading plus the alternative military loading specified by AASHTO for bridges on the Interstate system. An AASHTO Case I roadway was assumed for checking fatigue. The prototype bridge was also designed using improved elastic live-load lateral distribution factors generated using a three-dimensional finite-element model of the bridge. Live-load distribution factors developed for one lane loaded were used to check fatigue details for over 2,000,000 cycles for truck loading, as specified by AASHTO for a Case I roadway. The improved live-load distribution factors showed some significant reduction over factors computed using current AASHTO procedures, particularly for the interior girder. Details of the prototype bridge design may be found elsewhere (*10,11*).

Details of the model bridge design, fabrication, and erection have also been reported previously (*10,11*). The scale factor of 0.4 used for the model bridge was determined by physical characteristics of the FHWA Structures Laboratory, fabrication techniques, and availability of plate material. A typical cross section of the model bridge is shown in Figure 1, and an elevation view of one span is shown in Figure 2. Details of the model-bridge girders and precast panels are given below.

Girders

The top flange of each girder in the model bridge was ¼ in. by 5⅝ in. throughout. The web of each girder was ¼ in. by 27 3/16 in. throughout. The bottom flange of each girder was 9/16 in. by 8 in. throughout, except 11 ft 2 in. from the abutments where the flange thickness decreased to 5/16 in. All the above dimensions are nominal. Material tests were conducted on specimens taken from the actual plate material in the model to determine the static yield strengths of the webs, flanges, and stiffeners. Because it was desired to achieve average mea-

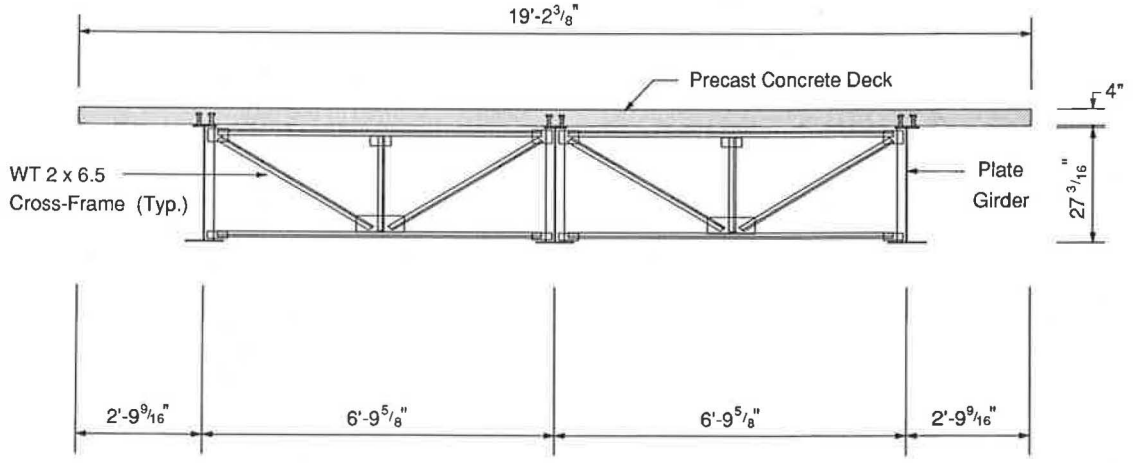

FIGURE 1 Cross section of model bridge.

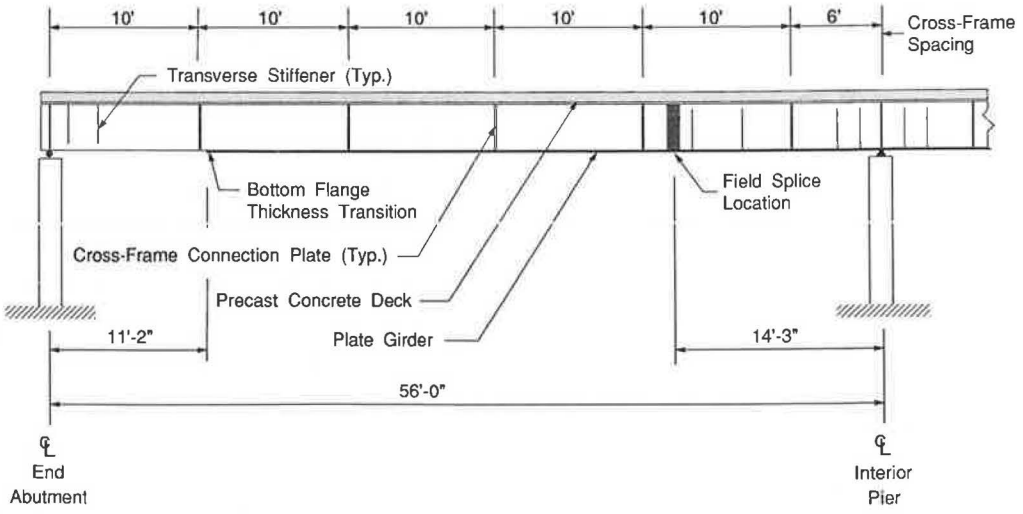

FIGURE 2 Elevation of model bridge.

sured static yield strengths as close as possible to the specified nominal yield strength of 50 ksi, and actual measured yield strengths are often higher than the specified nominal yield strength, ASTM A36 material was used for the girders. The average measured static yield strengths of the plate material used varied from 42.1 to 55.9 ksi.

Bearing stiffeners were located on both sides of the web of each girder over the supports. Cross-frame connection plates were located at 10-ft intervals, measured from the abutments, along the interior girder on both sides of the web and along each exterior girder on the inside face of the web only. This corresponds to a 25-ft cross-frame spacing in the prototype bridge, which is currently the maximum allowed by the AASHTO specification. Fillet welds were used to connect the cross-frame connection plates rigidly to the girder top and bottom flanges, as required by AASHTO. The cross-frames were composed of diagonals, top and bottom horizontal members, and a vertical post, all WT2 × 6.5 rolled sections. The cross-frame members were welded to ¼-in.-thick gusset plates, which were bolted to 5/16-in.-thick connection plates. Because only a limited number of rolled tee sections were available, the cross-sectional areas of the individual components of the cross-frames were not scaled down exactly from the prototype bridge. To evaluate the effect of improperly scaled down cross-frames, the stiffness of the cross-frame assemblages was varied in the finite-element model of the model bridge and found to have a negligible effect on the computed live-load distribution factors. Intermediate cross-frames were located 6 ft from each side of the interior pier. The cross-frames adjacent to the pier were spaced according to AI.FD criteria to brace the bottom (compression) flange and ensure adequate inelastic rotation capacity at maximum load.

Each girder had a bolted field splice 14 ft 3 in. on each side of the interior pier composed of ¼-in. splice plates fastened with ¾-in.-diameter ASTM A325 high-strength bolts. Each girder was supported on roller bearings at both abutments and on fixed bearings permitting rotation but no translation at the interior pier. Each end-abutment bearing was a 2-in.-diameter roller placed between two ¾-in. sole plates. The interior-pier bearing consisted of a ¾-in. sole plate, a plate with a rounded top surface, and two pintels. The top sole plates were welded to the bottom flange of the girders, and the bottom sole plates rested on circular load cells supported on concrete piers. The load cells were used to measure the girder reactions. Instrumentation on the steel girders included numerous strain gauges, deflection transducers, and rotation gauges.

Precast Panels

The 35 modular precast deck panels on the model bridge were each 4 in. thick, 3 ft 2 in. wide, and 19 ft 2⅜ in. long. The deck panels were pretensioned in the transverse direction using a 7/16-in.-diameter low-relaxation strand and posttensioned along the full length of the bridge after erection using a 0.60-in.-diameter low-relaxation strand. The bridge deck panels were designed on the basis of normal-weight concrete with a 28-day compressive strength of 6,000 psi. A "double-female" type of joint was used at the transverse panel-to-panel interface and grouted before posttensioning. After posttensioning, a 12-day waiting period was observed to allow for some of the concrete creep and shrinkage to occur before the panels were made composite with the girders. Grout was then placed in the 5/16-in. separation between the top of the girders and the bottom of the deck panels and in each pocket around the ⅝-in.-diameter, 3-in.-long stud shear connectors to achieve composite action. Leveling and hold-down devices were provided as specified in the prototype design. Two additional test panels were cast to obtain independent data on concrete creep and shrinkage. Instrumentation in the panels included strain gauges mounted on mild reinforcement bars embedded in the panels and numerous surface-mounted Whittemore points.

The average compressive strength of the concrete in the panels varied from 6,520 to 8,020 psi over the duration of the bridge tests. The average measured ultimate strength of the 7/16-in.-diameter prestressing strand was 281.7 ksi, and the average yield strength measured at 1 percent elongation was 247.8 ksi. The average measured ultimate strength of the 0.60-in.-diameter prestressing strand was 271.8 ksi, and the average yield strength measured at 1 percent elongation was 253.6 ksi. Measured yield strengths for both the 7/16-in.- and 0.60-in.-

diameter strands exceeded the minimum requirements for yield strength of 90 percent of the rated strand capacity for low-relaxation strands specified in ASTM A416.

Finite-Element Model

By using the general purpose finite-element program MSC/NASTRAN (*12*), a three-dimensional mathematical model of the model-bridge superstructure was generated. The three plate girders were modeled with three bar elements, one for the web and one for each flange. The three bar elements were rigidly connected to act as a single beam. A total of 40 grid divisions per span was used lengthwise along the model. The cross-frames were modeled with bar elements pinned at the ends to resist only axial loads.

The deck panels were modeled using four-node isoparametric plate elements that resist plane bending and membrane forces. Two plate elements were used transversely between each girder, and one plate element was used to model the deck overhang on one side of each of the exterior girders. Composite action was simulated by offsetting the flange and web bar elements from the concrete deck nodal points by the actual distance between them. It was assumed in the model that the concrete stiffness was fully effective throughout. A structural thickness of 10 in., a Poisson's ratio of 0.15, and a modulus of elasticity of 4,700 ksi were assumed for the deck-panel elements. Appropriate boundary conditions were input at each girder support.

COMPENSATORY DEAD LOADS

Because of the correct scaling of only the model-bridge geometry and applied loads, and not the weight density of the materials (concrete and steel), actual dead-load stresses in the model bridge were only about 40 percent of the computed dead-load stresses in the prototype bridge. To satisfy the rules of similitude, it was important to model critical dead-load moments and shears as closely as possible. Therefore, concentrated loads were applied to each girder at three locations in each span to simulate a compensatory uniform dead load. The loads were applied at approximately the 0.4, 0.6, and 0.8 point in each span of each girder, measured from the abutments. Noncomposite compensatory dead loads were applied to the bottom flanges of steel girders at these locations immediately after erection of the steel framing. These loads, applied to the noncomposite structure, compensated for the fact that the weight density of the steel girders and precast deck components in the model bridge could not be scaled correctly with a single linear scale factor. These noncomposite compensatory dead loads were maintained as constant as possible during erection of the deck panels.

Following erection, posttensioning, and grouting of the deck system, additional compensatory dead loads were applied to the composite structure. The composite dead loads were also applied to the bottom flanges of the girders and compensated for the loads due to the barrier curbs, railings, and future wearing surface that were included in the prototype design but were not physically present on the model bridge. Although it was recognized that elements such as parapets, curbs, and sidewalks may influence the distribution of live loads, it was beyond the scope of this research program to evaluate the possible effect of these elements, which was considered secondary compared with the effects of girder spacing, cross-frame spacing, and deck thickness.

The combined noncomposite and composite compensatory dead loads were maintained throughout the influence surface tests using a hydraulic loading system. After the service load tests, these loads were transferred from the bottom flanges of the steel girders to the top of the precast deck panels and maintained during the subsequent influence surface tests. A complete discussion of the compensatory dead-load system used may be found elsewhere (*10*).

INFLUENCE SURFACE TESTS

Lateral live-load distribution to the steel girders of the model bridge at elastic service load stress levels was evaluated by generating a series of influence surfaces for the bottom-flange axial force in each girder at selected locations. These bottom-flange forces were used as a measure of the bending moment in each girder. Deck-panel distribution behavior is not discussed here.

To generate the influence surfaces, a single concentrated load of 16.6 kips made of lead weights was applied to the top surface of the bridge deck at locations longitudinally spaced approximately every one-fifth of the span along the full length of the bridge. The magnitude of the load was selected so that measured strains could be recorded without causing yielding in the girders. The magnitude of the weight used is not related to an AASHTO wheel load or concentrated load. The lead weight was placed on two 4-in. by 12-in. wood blocks spaced 12 in. apart during testing. Figure 3 shows the lead weight used and the bearing blocks. In the transverse direction, the applied load was placed near the edge of the deck overhangs, directly over each girder, and halfway between the girders.

The elastic axial forces in the bottom flange of each girder caused by a single concentrated load placed at each location shown in Figure 4 were measured at the interior-pier section and at the approximate maximum positive-moment section of the west span. The line at the 0.4 point was assumed to be critical for bottom-flange axial forces in the positive-moment region, and the line at the 0.6 point was assumed to be critical for bottom-flange axial forces in the negative-moment region. Bottom-flange axial forces at each section were computed from the average of four measured strains at each bottom flange location. The measured forces were then used to compute critical elastic live-load distribution factors according to a method previously reported (*13*). To illustrate that lateral distribution factors vary along the span, distribution factors at critical positive-moment and negative-moment regions of the bridge for both interior and exterior girders were computed. Factors were computed for only one exterior girder, because the bridge is symmetrical. These factors were then compared with (a) factors computed from corresponding bottom-flange axial forces from a finite-element analysis of the model bridge using the same method, (b) factors computed using current AASHTO procedures, and (c) factors computed from proposed empirical formulas and recommendations

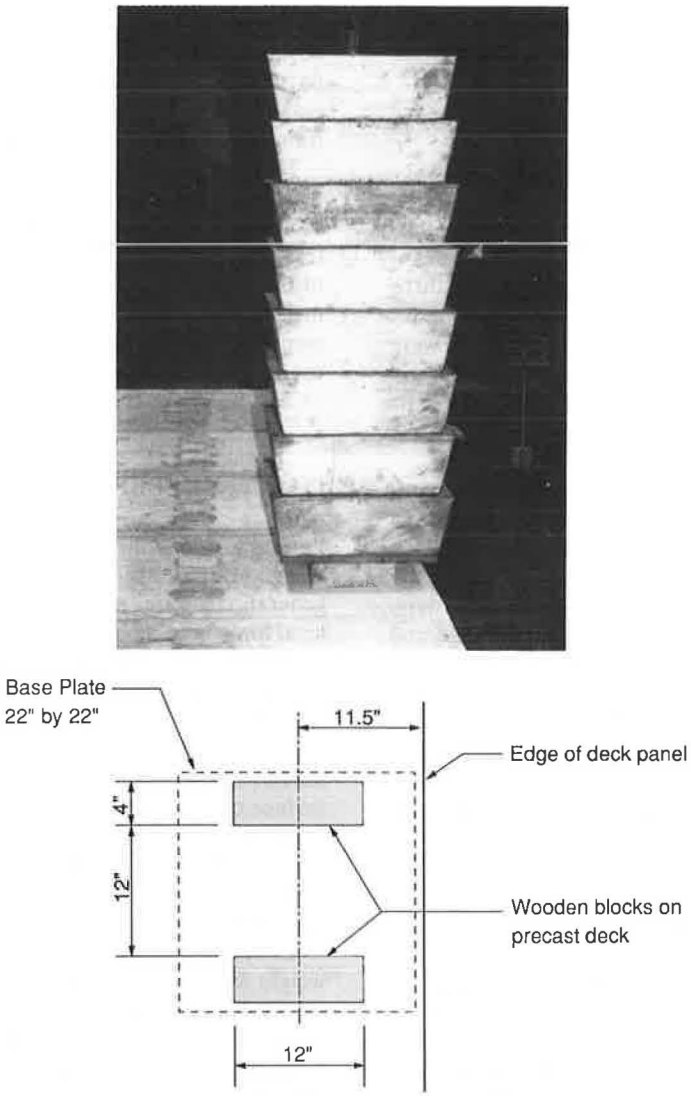

FIGURE 3 Details of dead weight for simulated wheel loadings.

developed in Phase I of NCHRP Project 12-26 on wheel-load distribution (*14*).

A series of three tests was conducted to develop influence surfaces for evaluation of the lateral live-load distribution to the girders in both positive-moment and interior-pier regions. The initial series of elastic influence surface tests, designated Test 1, was completed immediately following erection and instrumentation of the model bridge and application of the compensatory dead loads. In Test 1, all cross-frames in the model bridge remained in place.

Subsequently, the model bridge was subjected to multiple lanes of simulated AASHTO overload lane and truck loadings plus impact. The overload tests were designed to cause the formation of automoments and to illustrate shakedown under repeated loadings. After shakedown, the bridge behaves elastically again under subsequent loads not exceeding the initial overload (*1*). Permanent deformations due to controlled local yielding allowed at interior piers may be included in the dead-load camber. The stabilization of the controlled permanent deformations in the continuous steel girders during automoment formation and subsequent shakedown was observed and documented. The results of the overload testing were reported by Moore and Grubb (*11*). Following the completion of the overload tests, the second series of influence surface tests, designated Test 2, was conducted. The purpose of Test 2 was to evaluate the lateral live-load distribution to the steel girders after formation of the automoments and shakedown of the bridge. These lateral live-load distribution factors were compared with the distribution factors computed before the overload tests.

The third series of influence surface tests, designated Test 3, was conducted immediately following Test 2. For Test 3, selected intermediate cross-frames in the positive-moment regions of both the east and west spans were removed. The purpose of this test series was to evaluate the lateral live-load distribution to the girders with fewer cross-frames than required by the current AASHTO specification. In the west span, cross-frames designated D2–D5 (see Figure 4) were removed. In the east span, cross-frames designated D9–D12 (see Figure 4) were removed. The critical intermediate cross-frames adja

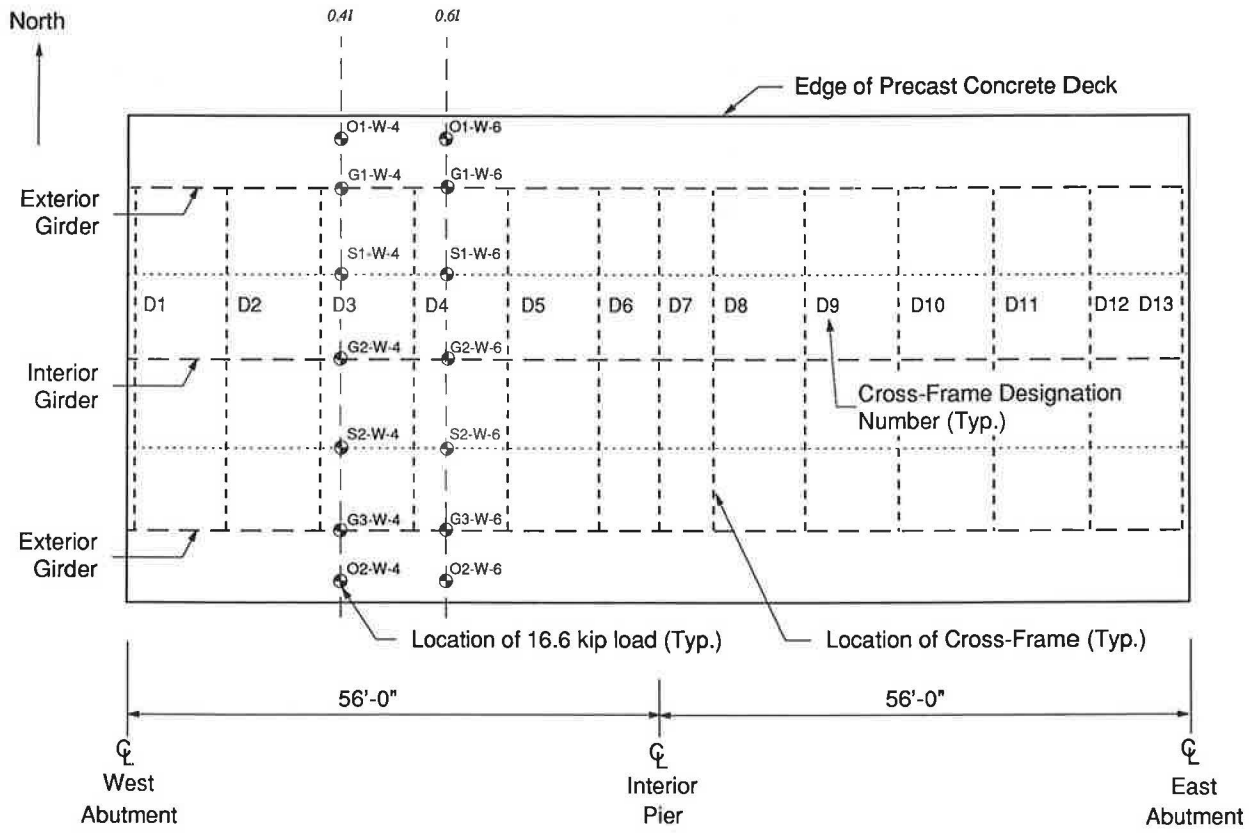

FIGURE 4 Plan view of model bridge showing the locations of the applied loads during the elastic influence surface tests.

cent to the pier, designated D6 and D8 in Figure 4, were not removed. These cross-frames brace the bottom (compression) flange in this region.

MEASURED BOTTOM-FLANGE AXIAL FORCES

Positive-Moment Region

To determine the critical distribution factors in the positive-moment region for each test, bottom-flange forces were computed from strains due to the 16.6-kip concentrated load measured at the 0.4 point of the west span (measured from the abutment) in the exterior and interior girders. The concentrated load was applied across the section at the 0.4 point in the west span. Figure 5 presents the bottom-flange forces in each test measured at the 0.4 point of an exterior girder in the west span for the loads applied across the section at the 0.4 point in the west span. Similarly, Figure 6 presents the bottom-flange forces in each test measured at the 0.4 point of the interior girder in the west span. Also shown in each figure are the corresponding bottom-flange forces from the finite-element model of the model bridge.

For the exterior girder, the bottom-flange forces in all three tests measured in the positive-moment region were generally within 10 percent of the bottom-flange forces predicted using the finite-element model. From Figure 5, no significant differences were observed in measured bottom-flange forces in the exterior girder at the 0.4 point for the tests completed before and after shakedown at overload, Tests 1 and 2. In addition, no significant differences were observed in measured bottom-flange forces in the exterior girder at the 0.4 point for the tests completed after shakedown with cross-frames in place and with selected cross-frames removed, Test 2 and 3.

For the interior girder, no significant differences were observed in bottom-flange forces measured at the 0.4 point for tests completed before and after shakedown at overload, Tests 1 and 2. When selected cross-frames were removed and the load was applied directly over the interior girder, the bottom-flange force in the interior girder measured at the 0.4 point increased 12 percent in Test 3 as compared with Test 2. For the load applied directly over an exterior girder, the bottom-flange force in the interior girder measured at the 0.4 point decreased 11 percent in Test 3 as compared with Test 2.

Negative-Moment Region

To determine the critical distribution factors in the negative-moment region for each test, bottom-flange forces were computed from strains due to the 16.6-kip load applied across the section at the 0.6 point of the west span measured at the interior pier in the exterior and interior girders (measured from the abutment). Figure 7 presents the bottom-flange forces in each test due to the application of the concentrated load across the section at the 0.6 point in the west span measured

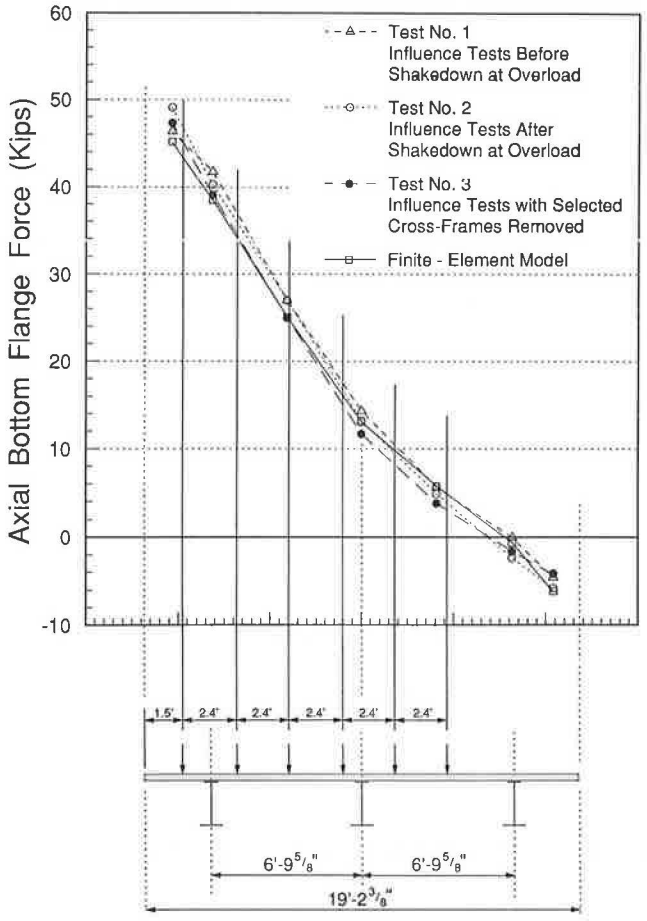

FIGURE 5 Comparison of bottom-flange forces at 0.41 (west span) from measured test data and the finite-element model for an exterior girder with the 16.6-kip load applied across the section at 0.41 (west span).

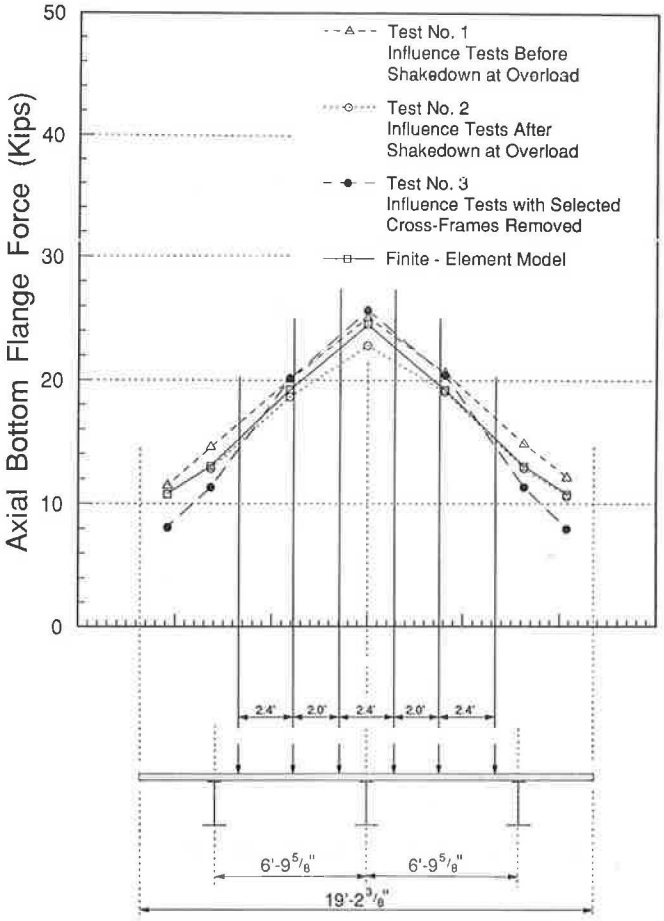

FIGURE 6 Comparison of bottom-flange forces at 0.41 (west span) from measured test data and the finite-element model for the interior girder with the 16.6-kip load applied across the section at 0.41 (west span).

at the interior-pier region of an exterior girder. Similarly, Figure 8 presents the bottom-flange forces measured in each test at the interior-pier region of the interior girder. Also shown in each figure are the corresponding bottom-flange forces from the finite-element model.

For both the exterior and interior girders, no significant differences were observed in bottom-flange forces measured at the interior pier in Tests 1 and 2, completed before and after shakedown at overload. For the case in which the load is applied directly over the interior girder, the bottom-flange force in the interior girder, measured at the interior pier, was approximately 24 percent higher in the test with selected cross-frames removed (Test 3) as compared with the test with all cross-frames in place (Test 2). For the load applied directly over an exterior girder, the bottom-flange force in the interior girder, measured at the interior pier, decreased 13 percent in Test 3 as compared with Test 2. In general, the bottom-flange forces predicted by the finite-element model underestimated the bottom-flange forces measured in each of the experimental tests.

DISTRIBUTION FACTORS

Once the plots discussed above were developed, the total bottom-flange axial force due to a single axle line of scaled-down AASHTO HS vehicles was computed for each location. [A single axle line had been determined to be sufficient in previous studies (*13*).] This scaled-down single axle line for three lanes of AASHTO HS vehicles is shown at the bottom in Figures 5–8. For each girder, the axles are shifted in their design lanes according to AASHTO rules to cause the worse loading on that girder. From each plot, contributing bottom-flange forces under each wheel were computed and summed for one, two, and three lanes loaded. Each wheel load was equal to the largest AASHTO HS scaled-down wheel load divided by 16.6. For three lanes loaded, the sum was reduced by 10 percent as allowed by AASHTO to account for the probability of coincident loading. Each sum was then divided by the theoretical elastic bottom-flange force at either the 0.4 point of the span or the interior pier, developed from a single-line-girder finite-element model loaded with the largest AASHTO HS scaled-down single axle load. The result was then multiplied by 2 to determine the corresponding distribution factor in units of wheels (*13*).

Wheel-load distribution factors for an exterior girder are summarized in Table 1. The distribution factors were computed using experimental data from each of the three tests and the method discussed above. In addition, Table 1 lists for comparison the wheel-load distribution factors computed using the same method with data from the finite-element model,

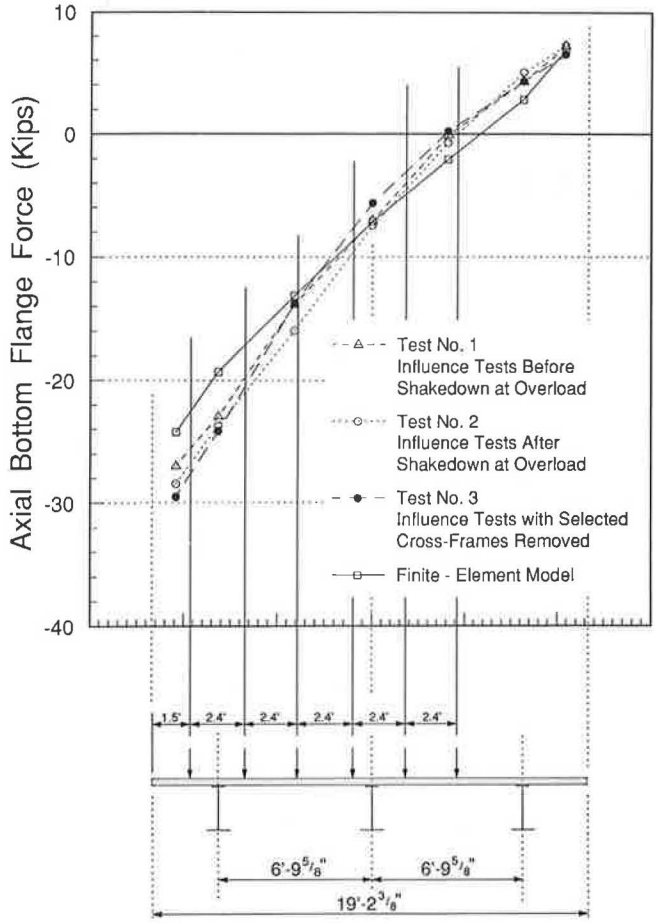

FIGURE 7 Comparison of bottom-flange forces at the interior pier from measured test data and the finite-element model for an exterior girder with the 16.6-kip load applied across the section at 0.61 (west span).

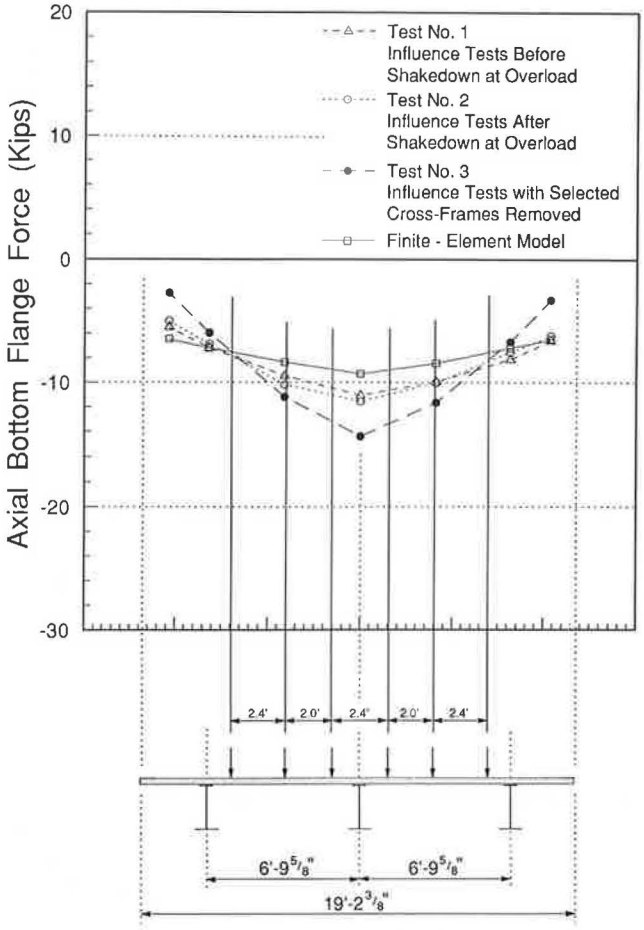

FIGURE 8 Comparison of bottom-flange forces at the interior pier from measured test data and the finite-element model for the interior girder with the 16.6-kip load applied across the section at 0.61 (west span).

factors computed according to the current AASHTO specification procedures, and factors computed from empirical formulas and recommendations proposed in NCHRP Project 12-26. The agreement between the factors computed from the experimental and finite-element analysis is well within 10 percent in the positive-moment region. For an exterior girder at the interior-pier region, the larger deviations of up to approximately 20 percent between the experimental and finite-element based factors appear to relate to some overestimation of the transverse stiffness of the model bridge by the elastic finite-element model. For the exterior girder, the current AASHTO provisions based on assuming the deck to act as a simple span between the girders provide wheel-load distribution factors that agree reasonably well with the experimental data, at least for more than one lane loaded. For multiple lanes loaded, the AASHTO factors were slightly conservative. It is recommended in the NCHRP Project 12-26 report (*14*) that this same approach be used for exterior girders until further research has been completed. According to the current AASHTO design-lane rules, a distribution factor cannot be computed for the case of three lanes loaded. As shown in Table 1, the observed slight variation in the distribution factor along the span is not considered in either the current AASHTO provisions or the proposed NCHRP formulas.

Table 2 summarizes similar data for the interior girder at both the positive-moment and interior-pier regions of the bridge. For the interior girder, factors computed on the basis of data from the three experimental tests and the finite-element analysis were well within 10 percent in the positive-moment region. Again, in the negative-moment region, the larger deviations of up to approximately 32 percent between the experimental and finite-element based factors appear to relate to some overestimation of the transverse stiffness of the model bridge by the elastic finite-element model. As with the exterior girder, the distribution factors for the interior girder vary slightly along the span of the bridge. For both the positive-moment region and the interior-pier region, the current AASHTO provisions produce very conservative distribution factors when compared with the factors computed on the basis of the experimental data and the finite-element analysis. On the basis of current AASHTO specifications, the deck is assumed to act as a simple span between girders because the girder spacing in the prototype exceeds 14 ft. The empirical formulas for interior girders proposed in NCHRP Project 12-26 for one lane loaded and for multiple lanes loaded produce distribution factors that are in close agreement with the experimental and finite-element data. The multilane formula proposed in NCHRP Project 12-26 does not differentiate between two and three lanes loaded.

TABLE 1 SUMMARY OF WHEEL-LOAD DISTRIBUTION FACTORS OF AN EXTERIOR GIRDER

	Positive - Moment Region			Interior - Pier Region		
	Number of Lanes Loaded			Number of Lanes Loaded		
	One Lane	Two Lanes	Three Lanes	One Lane	Two Lanes	Three Lanes
Experimental Results:						
Test No. 1 Influence Tests Before Shakedown at Overload	1.593	2.455	2.475	1.909	2.850	2.693
Test No. 2 Influence Tests After Shakedown at Overload	1.598	2.441	2.429	2.009	3.069	2.923
Test No. 3 Influence Tests with Selected Cross Frames Removed	1.538	2.309	2.274	2.025	2.915	2.706
Finite - Element Model	1.500	2.297	2.321	1.669	2.575	2.552
Current AASHTO Procedures	2.029	2.647	----	2.029	2.647	----
Procedures Proposed in NCHRP Project 12-26	2.029	2.647	----	2.029	2.647	----

---- denotes inapplicable

In NCHRP Project 12-26, limits of applicability were established for the proposed empirical formulas. The prototype bridge falls within the span-length limitation of 200 ft and the slab-thickness limitation of 12 in. However, it is important to recognize that other characteristics of the prototype bridge fall outside the limits of applicability for the empirical formulas proposed in NCHRP Project 12-26. The proposed formulas are only applicable to cross sections with four or more girders and a maximum transverse girder spacing of 16 ft. The model bridge tested in this research program was based on a prototype bridge utilizing only three girders and a transverse girder spacing of 17 ft. Nevertheless, the agreement between the experimental data and the proposed empirical formulas is quite good.

For both the interior and exterior girders in the positive-moment and interior-pier regions, the computed wheel-load distribution factors based on the influence surface tests conducted before and after shakedown at overload (Tests 1 and 2, respectively) varied less than 10 percent. In general, there was a trend for the distribution factors before shakedown to

TABLE 2 SUMMARY OF WHEEL-LOAD DISTRIBUTION FACTORS OF THE INTERIOR GIRDER

	Positive - Moment Region			Interior - Pier Region		
	Number of Lanes Loaded			Number of Lanes Loaded		
	One Lane	Two Lanes	Three Lanes	One Lane	Two Lanes	Three Lanes
Experimental Results:						
Test No. 1 Influence Tests Before Shakedown at Overload	0.909	1.642	2.122	0.881	1.663	2.154
Test No. 2 Influence Tests After Shakedown at Overload	0.832	1.499	1.940	0.921	1.693	2.211
Test No. 3 Influence Tests with Selected Cross Frames Removed	0.923	1.608	2.058	1.111	1.952	2.478
Finite - Element Model	0.880	1.555	2.008	0.748	1.421	1.879
Current AASHTO Procedures	1.647	2.824	2.806	1.647	2.824	2.806
Procedures Proposed in NCHRP Project 12-26	1.027	2.122	2.122	1.027	2.122	2.122

decrease slightly in positive-moment regions and increase slightly at the interior-pier regions after shakedown. This could be a result of some minor concrete cracking that may have occurred at the interior pier during the overload test.

In general, for both the interior and exterior girders, the distribution factors changed very little in the tests conducted after shakedown with the cross-frames in place and with selected cross-frames removed (Tests 2 and 3, respectively). For the case of the exterior girder in the interior-pier region, the computed distribution factors were reduced up to approximately 7.5 percent from the values after shakedown when the cross-frames were removed. For the case of the interior girder at the interior-pier region, the computed distribution factors increased an average of about 15 percent from the values after shakedown when the cross-frames were removed. These trends were slightly less pronounced in the positive-moment regions.

SUMMARY AND CONCLUSIONS

A large experimental test program has recently been completed to evaluate the behavior of a 0.4-scale model of a two-span continuous plate-girder bridge with precast prestressed modular concrete deck panels. The bridge, designed according to Alternate Load Factor Design (ALFD), or Autostress Design, procedures, utilizes noncompact plate girders with slender webs that fall beyond the current limits of the ALFD guide specification. A comprehensive test plan was followed to subject the model bridge to a series of tests designed to evaluate specific responses at simulated AASHTO service load, overload, and maximum load levels.

At elastic service-load stress levels, live-load lateral-distribution factors for the exterior and interior girders in positive and negative bending were computed from experimentally developed influence surfaces for the bottom-flange axial forces. These factors were compared with factors computed from a finite-element model, from current AASHTO procedures, and from proposed empirical formulas for interior girders. In positive-moment regions, the factors computed from the experimental and finite-element model data generally agreed within 10 percent. The larger deviations between the experimental and the finite-element model factors, in both interior and exterior girders, at the interior-pier region were probably caused by overestimation of cross-frame stiffness in the finite-element model. The interior-girder factors computed from the proposed empirical formulas also agreed reasonably well with experimental data, even though the prototype bridge used in this study falls outside the established range of applicability for the proposed formulas.

The factors computed using current AASHTO procedures were quite conservative for the interior girder, and less so for the exterior girders. The AASHTO factor for one lane loaded, used to check fatigue details for over 2,000,000 cycles of truck loading on Case I roadways, appeared to be extremely conservative in all cases. Neither the proposed nor the current AASHTO procedures accounted for the observed slight variation of the distribution factor along the span, but because the variation was small, this is probably justified. The data would seem to indicate that finite-element analysis is a plausible method for computing elastic wheel-load girder distribution factors. Also, the proposed empirical formulas appear to give reasonable results.

For tests conducted before and after shakedown at overload, the computed distribution factors varied less than 10 percent. This appears reasonable, because the bridge behaved elastically again after shakedown. The distribution factors before shakedown decreased slightly in postive-moment regions and increased slightly in negative-moment regions after shakedown, probably because of some minor concrete cracking that may have occurred over the interior pier during the overload testing. Thus, the data would seem to indicate that elastic distribution factors may still be used at overload, even though controlled local yielding is allowed in ALFD procedures.

For the tests conducted after shakedown with all cross-frames in place and with selected cross-frames removed, the computed distribution factors were generally reduced less than 7.5 percent in the exterior girders. For the interior girder, distribution factors increased up to an average of about 15 percent in negative-moment regions and an average of up to about 8 percent in positive-moment regions for the tests conducted with cross-frames in place and with selected cross-frames removed. However, the fact that the distribution factors did not vary significantly overall when the cross-frames were removed suggests that the load is primarily distributed through the concrete deck, at least for bridges without skewed supports.

ACKNOWLEDGMENTS

The work reported in this paper was part of a cooperative investigation sponsored by the Federal Highway Administration (FHWA) and the American Iron and Steel Institute (AISI). The study was conducted with the assistance of Sue Lane, Mary McGrath, and the staff of the FHWA Structures Laboratory. Additional assistance in testing the model bridge, reduction of test data, and data analysis efforts was provided by Pedro Albrecht and Kamal Elnahal of the University of Maryland and Chi Associates, Inc., Arlington, Virginia.

Design of the model bridge, load fixtures, instrumentation, and test plan was carried out by personnel from the steel industry and by Wiss, Janney, Elstner Associates, Inc. (WJE), retained by AISI to coordinate the technical aspects of the project. A. C. Kuentz of AISI and M. E. Moore of WJE served as co-principal investigators during the model bridge study. The staff of the study included M. A. Grubb of AISC Marketing, Inc.; R. P. Knight of Dynamic Isolation Systems, formerly of Bethlehem Steel Corporation; R. W. Lautensleger of ARMCO; and K. A. Strand of WJE.

The entire project was conducted under the guidance of an AISI Advisory Panel. The members of this panel were J. M. Barsom (Chairman) of U.S. Steel, a division of the USX Corporation; R. S. Fountain of Parsons-Brinckerhoff; G. Haaijer of the American Institute of Steel Construction; E. V. Hourigan of Parsons-Brinckerhoff, formerly of the New York Department of Transportation; C. L. Loveall of the Tennessee Department of Transportation; R. L. Mion of AISC Marketing, Inc.; B. T. Yen of Lehigh University; P. Zia of North Carolina State University; and I. M. Viest of Bethlehem, Pennsylvania.

Fabrication and erection of the model bridge was completed by Atlas Machine and Iron Works, Gainesville, Virginia. Precast components were fabricated by Shockey Bros. of Winchester, Virginia, and posttensioning was completed by VSL Corp., Springfield, Virginia. Load fixtures for the model bridge were fabricated by Salisbury Steel, Salisbury, Maryland.

REFERENCES

1. G. Haaijer, P. S. Carskaddan, and M. A. Grubb. *Suggested Autostress Procedures for Load Factor Design of Steel Beam Bridges*. Bulletin 29. American Iron and Steel Institute, Washington, D.C., April 1987.
2. *Guide Specification for Alternate Load Factor Design Procedures for Steel Beam Bridges Using Braced Compact Sections*. American Association of State Highway and Transportation Officials, Washington, D.C., 1986.
3. M. K. Elnahal, P. Albrecht, and L. R. Cayes. *Load Distribution in a Two-Span Continuous Bridge*. Report FHWA-RD-89-101. FHWA, U.S. Department of Transportation, June 1989.
4. A. Vasseghi and K. H. Frank. *Static Shear and Bending Strength of Composite Plate Girders*. Final Report AISI Project 320A, Phil M. Ferguson Structural Engineering Laboratory Report 87-4. University of Texas, Austin, June 1987.
5. C. G. Schilling. *Moment-Rotation Tests of Steel Bridge Girders*. AISI Project 188. American Iron and Steel Institute, Washington, D.C., April 1985.
6. C. G. Schilling. *Exploratory Autostress Girder Designs*. AISI Project 188. American Iron and Steel Institute, Washington, D.C., July 1986.
7. C. G. Schilling and S. S. Marcos. *Moment Rotation Tests of Steel Girders with Ultracompact Flanges*. AISI Project 188. American Iron and Steel Institute, Washington, D.C., July 1988.
8. C. G. Schilling. *A Unified Autostress Method*. AISI Project 51. American Iron and Steel Institute, Washington, D.C., Nov. 1989.
9. *Standard Specifications for Highway Bridges*, 13th ed. American Association of State Highway and Transportation Officials, Washington, D.C., 1986.
10. M. E. Moore and I. M. Viest. Laboratory Tests of a Continuous Composite Bridge. In *Proceedings of Conference on Composite Construction in Steel and Concrete*, Henniker, N.H., American Society of Civil Engineers, New York, June 1987.
11. M. E. Moore and M. A. Grubb. Behavior of a Two-Span Continuous Plate Girder Bridge Designed by the Alternate Load Factor Method. In *Proceedings of the National Engineering Conference*, Nashville, Tenn., American Institute of Steel Construction, Chicago, Ill., 1989.
12. C. W. McCormick. *MSC/NASTRAN User's Manual*. MacNeal-Schwendler Corporation, Los Angeles, Calif., April 1982.
13. P. S. Carskaddan and M. A. Grubb. *Live-load Lateral Distribution for the Approach Spans for the Cooper and Wando River Bridges*. U.S. Steel Research Bulletin. U.S. Steel, June 1983.
14. R. V. Nutt, R. A. Schamber, and T. Zokaie. *Distribution of Wheel Loads on Highway Bridges*. Final Report, NCHRP Project 12-26. TRB, National Research Council, Washington, D.C., April 1988 (available on a loan basis from NCHRP).

Publication of this paper sponsored by Committee on Steel Bridges.